Bilayer graphene interface with a Quantum Twisting Microscope

Alejandro Martín

Supervised by: Prof. Carmen Rubio Verdú

ICFO, Spain.

25 August 2024

Moiré physics, which studies the novel properties that arise when two or more 2D crystals are stacked with a twist between their layers, has unveiled unique electronic, optical, and mechanical properties, revolutionizing condensed matter physics. This thesis explores the use of the Quantum Twisting Microscope (QTM) to investigate the electronic properties of twisted bilayer graphene with in-situ control over the twist angle. The QTM is a novel scanning probe that enables dynamic rotation of 2D crystals, something unachievable before the development of the technique. The primary objective of the current work is to demonstrate our QTM's capabilities in conducting in-situ twistronics experiments and detail the fabrication methods required for it. The experimental setup includes our own QTM which is created by adapting a commercial Atomic Force Microscope (AFM). The main modifications are a unique van der Waals tip and a modified sample stage that allows for twist angle control between the tip and sample. Our experience has demonstrated the importance of maintaining high quality standards in the fabrication of tips and samples to ensure succesful experiments. The main result of this thesis is the development of the fabrication techniques needed to achieve highly-clean surfaces in both parts of the QTM. This achievement has allowed us to reproduce previously reported behavior of the conductance across a twisted bilayer graphene interface. The successful implementation of our setup demonstrates its potential as a powerful tool for exploring moiré physics and engineering novel quantum states in 2D materials.

Keywords: 2D materials, Moiré materials, Quantum Twisting Microscope, Twistronics, Twisted bilayer graphene.

Alejandro Martín: alejandro.martin@icfo.eu

Contents

1 Introduction

The discovery of two-dimensional (2D) materials has revolutionized condensed matter physics, uncovering a wide array of novel electronic, optical, and mechanical properties. One of the most recent and intriguing phenomena in this field is moiré physics, which can emerge when two or more 2D crystals are stacked with a slight twist between their layers. This twist leads to the formation of moiré patterns, drastically altering the electronic properties of the materials. The ability to manipulate the twist angle precisely has opened up new opportunities for engineering exotic states of matter such as unconventional superconductivity [1], fractional Chern insulators [2], or Wigner crystals [3, 4], among others.

Interestingly, the physics associated with moiré patterns are highly dependent on the twist angle and achieving high-precision control over this degree of freedom has posed significant challenges. Traditional methods for fabricating twisted materials are tricky and time consuming. Moreover, the complexity of the methods burdens the reproducibility and systematic study of this new tuning knob. In the end, this has limited the ability to fully explore the potential of moiré systems.

The development of the Quantum Twisting Microscope (QTM) [5] marks a significant breakthrough in this field. The QTM is a new kind of Scanning Probe (SP) technique that allows for a dynamic and precise control of the twist angle between two 2D crystals, something that was previously unachievable. This capability enables in-situ twistronics experiments, where the electronic properties of the materials are continuously measured as the twist angle is modified. This innovative technique provides an unprecedented platform to study the behavior of electrons in twisted systems, paving the way for new discoveries in condensed matter physics.

In the current work, we explore the capabilities of the QTM to perform in-situ twistronics experiments and detail the fabrication methods needed to carry them out. To the best of my knowledge, our QTM is the second one in the world to be operational. Given the novelty of the technique, we have faced many challenges to achieve this landmark.

The thesis is structured as follows: **Section 2** provides an overview of the necessary background to understand the revolution introduced by the QTM. **Section 3** details the experimental setup and methodology, including the fabrication of the QTM's unique van der Waals tip, which is crucial for forming pristine 2D junctions. **Section 4** presents the results of our in-situ twistronics experiments on twisted bilayer graphene, demonstrating the QTM's capability to dynamically tune electronic properties and observe phenomena such as coherent tunneling between the layers. Moreover, we discuss the challenges faced during the fabrication of high-quality tips and samples. Finally, **Section 5** outlines potential future directions for research and improvements in the QTM technique.

The QTM is a revolutionary tool that not only enhances our ability to study the electronic properties of 2D materials but also opens new avenues for discovering and engineering novel quantum states. By enabling the dynamic rotation of 2D crystals, the QTM offers a unique platform for probing highly angular dependent moiré physics such as the interlayer conductance of twisted bilayer graphene.

2 Background

2.1 Layered materials and vdW heterostructures

Layered materials are a class of materials characterized by presenting strong covalent bonds with their in-plane neighbors and weak van der Waals (vdW) interactions with the out-of-plane atoms. This unique bonding structure allows for the mechanical exfoliation of individual layers, resulting in atomically thin two-dimensional (2D) crystals.

The first ever 2D material to be isolated was graphene [6]. As it was theoretically predicted, the mechanical, optical and electronic properties of the mono layer were found to be drastically different to its 3D counterpart (graphite). For instance, graphite is a good metal while mono layer graphene (MLG) is a semi-metal. Shortly after graphene was discovered, other materials were mechanically exfoliated: hexagonal boron nitride (hBN), tungsten disulfide (WS_2) or niobium diselenide ($NbSe_2$), the last two being Transition Metal Dichalcogenides (TMDs). Even tough all of them were atomically thin crystals, their properties were completely different:

- **Graphene:** Is a semi-metal whose atoms are arranged in a honeycomb lattice (see Figure 1a). In reciprocal space, this crystalline structure is also an hexagon whose vertices are commonly refer to as K and K' points (see Figure 1b). A simple tight binding model of graphene (Figure 1c), shows that electrons experience a linear dispersion near the K points. The band structure created at these points is called a Dirac cone and is responsible for many of the interesting phenomena present in graphene, such as high electron mobility and the quantum Hall effect [7].
- **hBN:** Similar to graphene, the atoms in hBN are arranged in a honeycomb structure but with different chemical species in each sublattice: boron and nitrogen. This key difference introduces a bandgap in the electronic structure, making hBN an excellent insulator. Its wide bandgap and chemical stability makes hBN an ideal substrate for graphene-based electronics and other 2D material devices.

The field of 2D materials becomes even richer when we combine these crystals at will. The weak vdW forces that enable the exfoliation, are also sufficiently strong to hold these layers together when they are placed or stacked on top of each other. This fact allows for the creation of artificial structures commonly called **vdW heterostructures**. In these

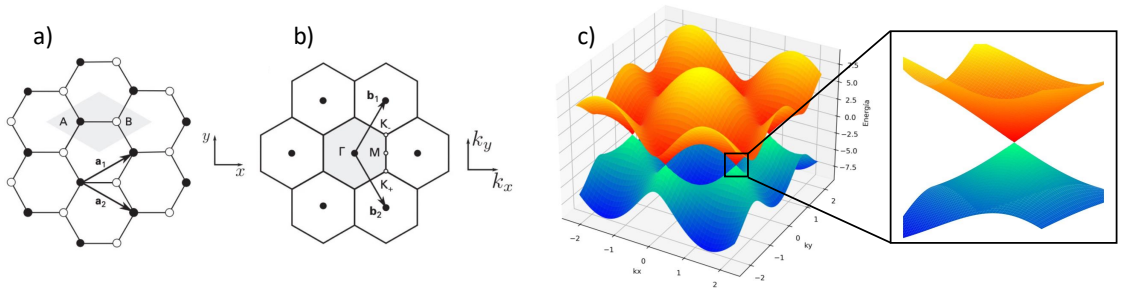

Figure 1: a) Real space honeycomb lattice, where A and B denote two inequivalent atoms. In graphene they are both carbon atoms. In hBN one is boron and the other nitrogen. In hBN, atomic distance is 1.5% shorter than in graphene. b) Reciprocal space lattice, showing the K^+ and K^- points in the first Brillouin zone. c) Band structure of graphene. The inset represents a close up near one of the K points showing the linear dispersion. a and b figures are adapted from [8]

systems, one can enhance the intrinsic properties of the materials or even engineer new behavior not present in the separate crystals. For example, by encapsulating graphene with hBN and using a graphite flake as bottom gate, one can obtain an unprecedented electron mobility [9]. Similarly, by stacking WSe_2 [10] with graphene, one can induce spin-orbit coupling to the system.

2.2 Moiré quantum matter

In 2018, a new revolution in condensed matter physics was sparked by the discovery of correlated insulator states [11] and unconventional superconductivity [1] in Magic Angle Twisted Bilayer Graphene (MATBG), a device made of two graphene layers rotated exactly 1.1°. This breakthrough has opened up a new field where engineering new properties is possible by creating interference patterns within 2D crystals. The new patterns that arise are called **moiré superlattices**, and their appearance can lead to a drastic modification of the host material. There exist two possibilities to create a moiré pattern (see Figure 2):

- **Lattice Mismatch:** Stacking two 2D crystals with slightly different lattice constants results in a moiré pattern.
- **Twist angle:** Rotating one layer relative to another by a small angle also creates a larger periodic structure.

The appearance of interesting phenomena in moiré systems was theoretically envisioned due to the formation of flat bands. These flat bands enhance electron-electron interactions, due to their reduced bandwidth, and facilitate the emergence of correlated physics [12].

However, experimentally studying moiré materials presents significant challenges. Fabricating twisted heterostructures requires precise control over the twist angle and maintaining the desired angle across the entire sample, known as angle homogeneity. Additionally, relaxation effects, induced stress, and other mechanical deformations can influence the properties of the moiré superlattice [13]. These complexities add multiple degrees of freedom that must be carefully managed to explore the full potential of moiré materials. Despite these challenges, ongoing advancements in fabrication techniques and experimental methods continue to push the boundaries of what can be achieved with these intriguing systems.

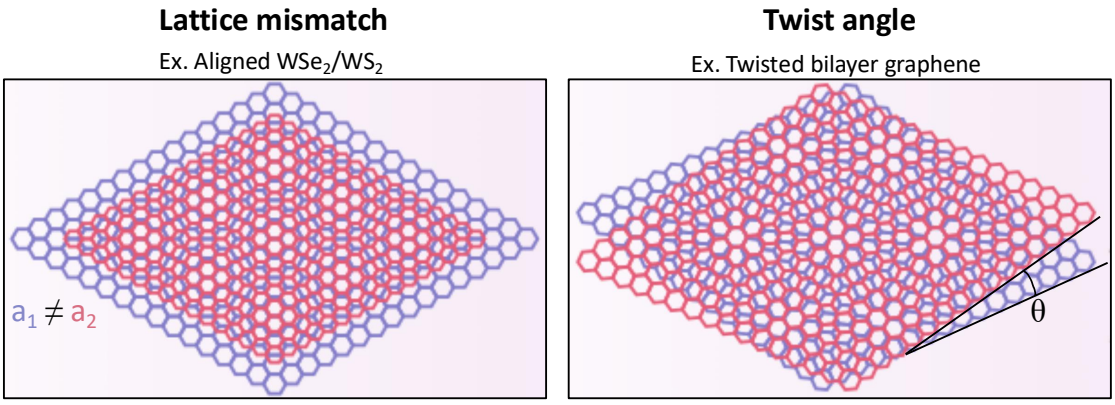

Figure 2: Schematic diagram of the formation of moiré patterns due to lattice mismatch of the components (left) and relative twist angle (right). In both of them, a larger periodic structure forms with a characteristic length scale associated to the distance between equivalent points. Adapted from [14].

2.3 Scanning probe techniques

Scanning Probe Microscopy (SPM) is a powerful family of techniques used to study the properties of materials at the micro and nanoscale. By using a probe that scans across the sample's surface, SPM provides detailed information about a material's topography or electronic structure. The primary advantage of SPM is its ability to access and measure locally with high spatial resolution, made possible by the precise control over the position of the probe. All SPM techniques share a common operational principle: the probe is brought very close to the sample, and an interaction is measured as the probe scans across the surface. This interaction can be a tunneling current, a force, or static charge among others, depending on the SPM technique. Common SPM techniques include Scanning Tunneling Microscopy (STM) [15], Atomic Force Microscopy (AFM) [16], and Scanning Near-field Optical Microscopy (SNOM) [17], each providing unique insights into the material being studied by measuring different interactions.

Moiré materials exhibit periodic modulations in their properties, such as charge localization, that are larger than atomic distances but much smaller than the overall sample's size. For this reason, SP techniques are ideal for studying these systems. They provide the necessary resolution to unveil quantum phases that remained hidden to spatially averaged global techniques, such as magneto-transport measurements. Given its close relation to this work, I will briefly describe the operating principle and morphology of an AFM.

2.3.1 Atomic force microscope

An Atomic Force Microscope (AFM) operates by scanning a sharp tip (see Figure 3a) over the sample's surface and sensing the interatomic force between the tip's apex and the sample. The forces between the tip and the sample cause the cantilever to deflect, and this deflection is measured using a laser beam reflected off the top of the cantilever into a photodetector (see Figure 3b). Additionally, a feedback control is activated to maintain a constant force. The resulting scan provides a high-resolution map of the sample's topography and can also be used to measure mechanical properties.

Consequently, one of the key strengths of an AFM is the precise control over the relative XYZ position between the tip and sample. Building upon this precise positioning capability, AFM cantilevers have been used in the few works [18, 19] that have achieved in-situ control over the twist angle of layered materials.

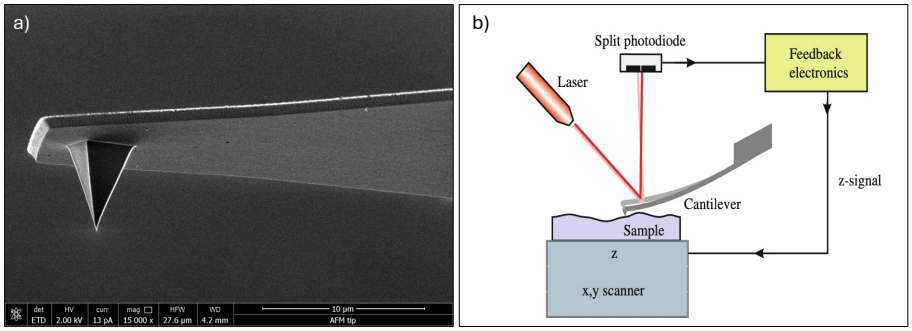

Figure 3: a) SEM image of a commercial AFM cantilever. b) Basic scheme to perform AFM topographic images. Adapted from [20]

2.4 Previous work on twistable interfaces

The investigation of twisted 2D materials has garnered significant interest due to the novel electronic properties that emerge in these systems. Traditional scanning probes serve solely as measuring instruments and cannot alter the sample itself, which is a significant limitation in the study of moiré systems. Over the past few years, researchers have developed experimental setups capable of inducing rotation between layered materials, enabling preliminary exploration of the resulting electronic phenomena. Two experimental works stand out:

Rotated graphite-graphene contacts. One notable study by Chari *et al.* [19] investigated the resistivity of rotated graphite-graphene contacts. They fabricated cross-shaped devices where a single-crystal graphite contacted a MLG (see Figure 4a). Using an AFM tip, they applied torque to change the relative orientation between the graphite and graphene. They found that the contact resistivity exhibited a 60° periodicity corresponding to the crystallographic symmetry of graphene and observed sharp dips in resistivity around 22° and 39° (see Figure 4b).

This work represented a promising advancement in developing twistable devices but faced limitations such as the inability to dynamically control the twist angle and issues with mechanical stability. Additionally, the technique was limited to rotating graphene-graphite interfaces. These facts highlighting the need for new developments that offered continuous control and the capability to create other interfaces.

Interface between misoriented graphite crystals. A similar study by Koren *et al.* [18] explored the electrical transport across graphite crystals with continuous control over the rotation angle. They fabricated cylindrical pillars of Highly Oriented Pyrolytic Graphite

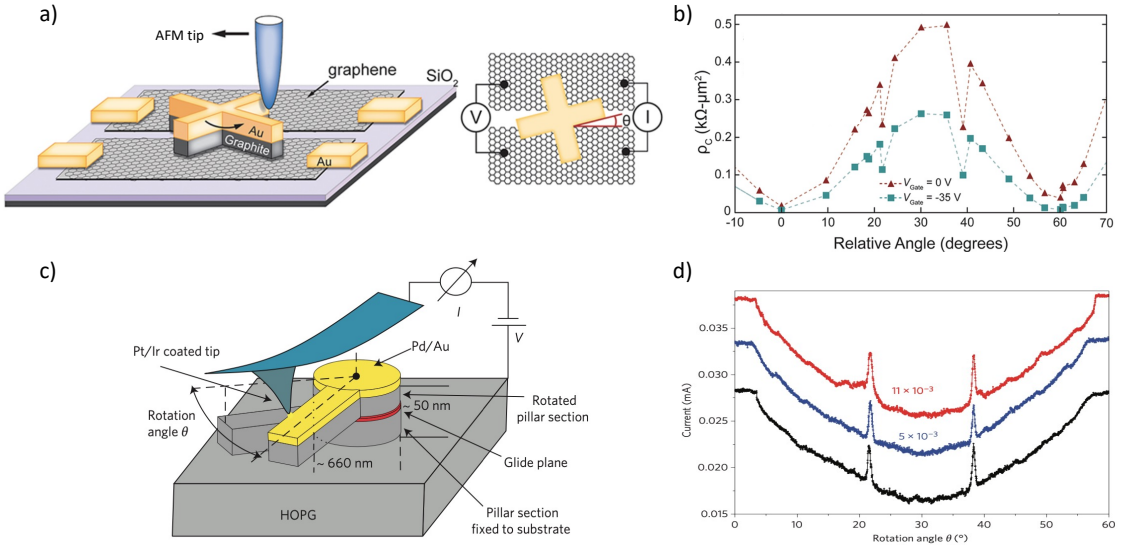

Figure 4: **Experimental setups for studying twistable interfaces.** a) Schematic of the AFM-based approach used in [19] to rotate a graphite structure relative to a MLG. b) Experimental result of the resistivity measured in the graphite-graphene contacts as function of the relative angle. c) Detailed view of the lever arm mechanism used in [18] to induce rotation to the HOPG pillar. d) Measured current flowing through the HOPG structure at a bias potential of V = 50 mV while continuously rotating the lever arm. Three independent data samples obtained from different pillar structures are shown.

(HOPG) equipped with a lever arm (see Figure 4c). Using an AFM tip, they applied a horizontal force to the lever arm, inducing rotational movement within the HOPG pillar. They observed an overall 60° periodicity in the conductance and sharp peaks at 21.8° and 38.2° (see Figure 4d)[1]. The conductive behavior was consistent with phonon-mediated interlayer transport, and the peaks were attributed to the formation of a coherent 2D electronic interface state.

This study achieved several key advancements, such as allowing continuous rotation of the interface and identifying the nature of the key features of the conductance as a function of the twist angle. However, reproducibility was not optimal as each pillar could only be used once. Moreover, the rotation happened between graphite crystals, so the challenge of rotating individual 2D layers was still unmet.

The studies discussed above have laid a crucial foundation for in-situ investigation of the twist angle. However, they also highlighted significant limitations. These challenges underscored the need for a more sophisticated approach that could offer precise, in-situ control over the twist angle between 2D crystals. This need has been addressed by the development of the Quantum Twisting Microscope (QTM) [5], a completely new Scanning Probe technique that leverages the strengths of traditional AFM technology and introduces innovative features to overcome these limitations. The QTM represents a significant advancement in the study of moiré systems, enabling continuous and precise manipulation of 2D crystals and opening new avenues for exploring their unique electronic properties.

3 Materials and methods

3.1 The Quantum Twisting Microscope

The Quantum Twisting Microscope (QTM) integrates a completely innovative probing tip and an advanced rotation mechanism, allowing it to dynamically rotate two different 2D crystals while performing measurements. This groundbreaking technique opens new possibilities for studying moiré materials.

The QTM's probe elevates and AFM tip to become a crucial part of the twisted system. In our case, the twisted device is separated into two: a standard vdW heterostructure sitting on a flat surface and another vdW heterostructure laid on a platinum pyramid allocated on a tip-less AFM cantilever (see Figure 5a and b). With this approach, we are able to create a pristine 2D plateau at the apex of the pyramid.

Thanks to the precise XYZ control inherited from the AFM, one can bring the tip and sample into contact with high accuracy (see Figure 5c). The contact area combines both heterostructures to become a completely new 2D device. Additionally, the sample stage of the original microscope is modified to accommodate a piezoelectric rotator and XY nanopositioners. This setup allows rotational control of the sample as well as positioning the center of rotation right at the junction point. Moreover, the AFM's feedback control ensures a constant force between the tip and sample along the entire experiment.

[1]Recall that Figure 4c plots the resistivity on the junction while Figure 4d plots the current (or conductance) of the junction, one is the inverse of the other one.

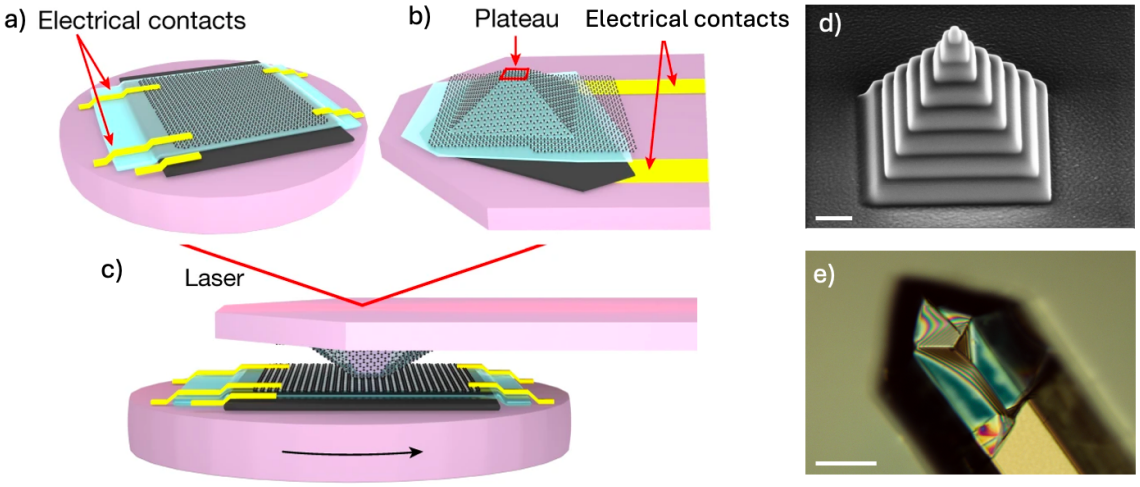

Figure 5: a) Sample formed of a vdW heterostructure on an artificial cliff. The top layer represents a MLG that is electrically connected. The blue layer is hBN. The black layer is a graphite flake that is also electrically connected. b) QTM tip formed by a vdW heterostructure dropped on Pt pyramid at the edge of a tip-less AFM cantilever. At the apex of the pyramid, a spontaneous plateau is formed. The layers are the same as in (a). c) Contact position to perform in-situ twistronics experiments. The sample rests on a rotatable stage. A constant force is maintained by using the laser control of the original AFM. Adapted from [5]. d) SEM image of the Pt pyramid built on the tip-less AFM cantilever. Scale bar is 400 nm. e) Optical image of a functional QTM tip. Scale bar is 50 μm.

The main revolutionizing factor of the QTM is the creation of the **vdW tip**. This new probe starts as a tip-less AFM cantilever where a platinum pyramid is built close to its edge. This pyramid is approximately 2 μm wide/long and 1.5 μm tall, and it is obtained by electron beam deposition (see Figure 5d). On top of the pyramid, a vdW heterostructure (or *stack* as I may refer to it occasionally) is dropped from a polymer film (see Section 3.2 for details). The stack is formed by three layers: graphite-hBN-active vdW material 1 (typically MLG):

- **The top layer** is one of the materials under study and it is half of the twistable interface. This layer must have an electrical connection.
- **The hBN** acts as an insulating layer as well as a flat substrate for the active crystal to lay on.
- **The graphite** serves two functions: as a flexible canvas to facilitate the formation of a tent-like shape (see Figure 5e) and as a possible top gate to the device. If the graphite serves as gate, it must have a separate electrical connection. When this is not case, the graphite is typically short-circuited with the active layer.

The second half of the twistable interface, **the sample**, is a another stack of vdW materials sitting on a 40 μm tall artificial cliff. In the most basic configuration, the stack has two layers: hBN-active vdW material 2:

- **The top layer** is the active material and the second half of the twistable interface. It must have an electrical connection.
- **The hBN** acts once again as a insulating layer that enhances the intrinsic properties of the active layer.

- It is also possible to add a **graphite** flake at the bottom to act as a bottom gate to the device. In this case, it must also have a separate electrical connection.

Two type of experiments have already been realized with a QTM: **in-situ twistronics** and **momentum resolved tunneling spectroscopy**. In this thesis we have focused on the first kind.

3.1.1 In-situ twistronics

With the in-situ twistronics configuration, we can now study an interface that remained elusive until this machine was developed: a twistable real bilayer. While the active materials of the tip and sample can differ in the most general case, this work focuses on a MLG tip and a MLG sample. This creates, at the junction, a twistable bilayer graphene. Figure 6 shows a schematic cross section of the junction with the corresponding circuit components to perform the experiment. A bias voltage V_b is applied between the tip's and sample's MLG and the current flowing through the junction is continuously measured as the rotation is controlled. If desired, top V_{TG} and bottom V_{BG} gate voltages can be applied to the top and bottom graphite flakes. Using this configuration allows us to control the local carrier density as well as the electric field at the twistable interface.

Controlling the twist angle is crucial because it allows us to systematically explore the electronic properties that emerge at different angles with unprecedented resolution ($\approx 0.01°$). Additionally, applying top and bottom gate voltages to the graphite flakes allows us to explore the phase diagram of the twisted device. This level of control is essential for tuning the electronic states.

The size of the junction depends on the dimensions of the plateau, which is correlated to the thicknesses of the top graphite and hBN layers. In our case, asymmetric triangular plateaus form, whose longer side is usually several hundred nanometers. This is much larger than the apex of the pyramid. Which means, as addressed by Inbar *et al.* [5],

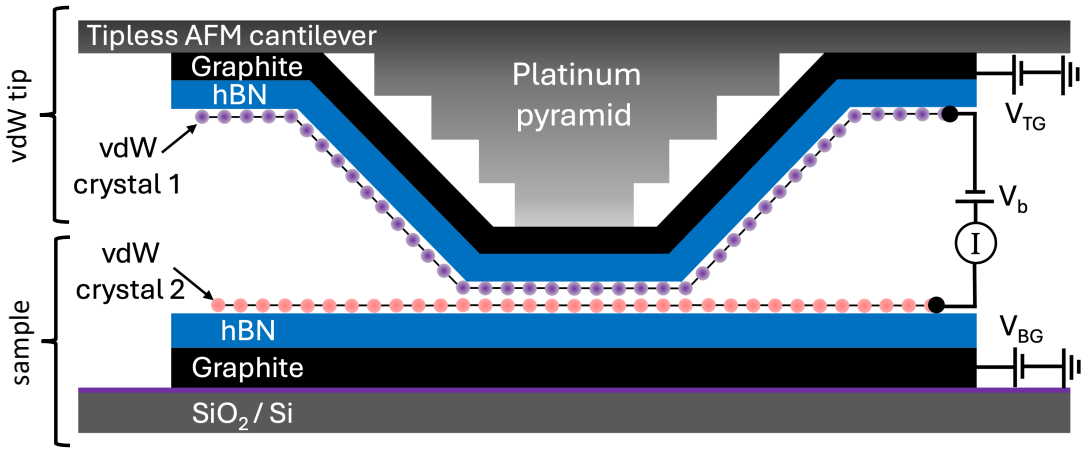

Figure 6: Schematic cross section of the QTM junction in a in-situ twistronics experiment. Two separate components can be distinguished. i)The probing tip: formed by a three layers heterostructure laid on a Pt pyramid that is built on a tipless AFM cantilever. ii)The sample: a three layers heterostructure laid on a artificial cliff created on a SiO_2/Si substrate. Both components are in contact and a bias voltage (V_b) is applied between the top layers while the current is measured. Additionally, top and bottom gates (V_{TG} and V_{BG}) are applied to the top and bottom graphite flakes. Image not to scale.

that the heterostructure uses the apex as a pivotal point with the rest of the stack hanging without touching the pyramid. These dimensions are small enough to consider the pyramid a probing tip, but large enough to hold many atoms and accurately assume that we have an MLG at the plateau.

3.1.2 Data acquisition setup

The data acquisition setup for the in-situ twistronics experiments is illustrated in Figure 7. This setup includes the following components:

- **Twistable interface**: The core of the setup is the twistable bilayer graphene formed between the tip and the sample. The tip's and sample's graphene have independent electrical connections that are connected to a coaxial cable.
- **Bias Voltage Application**: An AC bias voltage $V_b(t, \omega_{\text{ref}})$ is generated by the lock-in amplifier. This bias voltage, with a specific reference frequency ω_{ref}, is applied to the junction. As a result, an AC current $I_{sig}(t, \omega_{noise})$ is induced. This current contains the signal with ω_{ref} but also noise components.
- **Current-to-Voltage conversion**: The current signal is fed into a pre-amplifier, which converts it into a voltage signal $V_{\text{sig}}(t, \omega_{\text{noise}})$ and amplifies it by a factor of 100.
- **Lock-in Amplifier**: The amplified voltage signal is then fed into the lock-in amplifier. It uses the reference frequency of the applied bias voltage to isolate the desired signal from the noise. This is achieved through a process called Phase-Sensitive Detection (PSD), where the lock-in amplifier multiplies the incoming signal by a reference signal and filters out the high-frequency components (see Appendix A for details). This filtering effectively removes the noise, leaving a clean measurement of the current through the junction.

3.2 Fabrication

In this section I will describe the entire process to obtain the two main components of the QTM: the **tip** and the **sample**. Both devices are addressed separately and the success of the experiments relies on achieving high quality standards in both parts. In summary, the steps are the following.

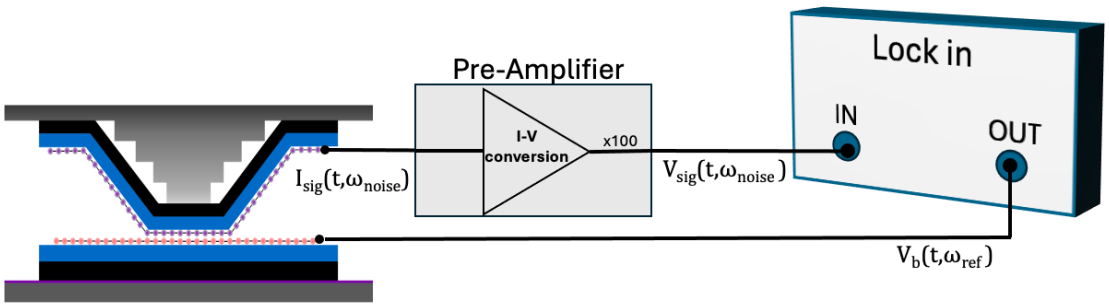

Figure 7: Schematic representation of the data acquisition instrumentation for in-situ twistronics experiments.

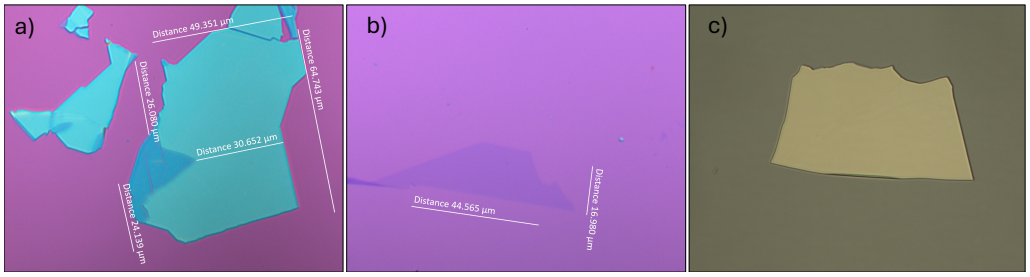

Figure 8: (a)hBN on SiO_2, (b) graphene on SiO_2 and (c) graphite on PPC.

For the **sample side**: Firstly the sample stage must be made. Starting from a SiO_2 substrate and using lithography+etching techniques, we design the sample stage's geometry. Secondly, the sample heterostructure is obtained by stacking the different materials. Thirdly, the stack is dropped down on the sample stage and the chip is vacuum annealed for cleaning. And lastly, Cr/Au contacts are evaporated using a hard masks.

For the **tip side**: Starting from a tip-less AFM cantilever, a Pt pyramid is built by e-beam deposition. Then, the heterostructure is fabricated and dropped on top of the pyramid. Later, the device is annealed to get rid of the polymer, and lastly, the electrical contacts are evaporated using a hard mask. It is also possible to evaporate the Cr/Au on the cantilever surface before building the pyramid.

3.2.1 Preparations to make a stack: heterostructure design and stamp fabrication

In this subsection I will briefly introduce the preparatory steps to make a vdW heterostructure. The process starts with the **exfoliation** of the components. This is the action of going from a bulk crystal with hundreds of thousands of layers, to very thin ones, aiming for the monolayer limit in the case of graphene. We need to exfoliate the different materials that will form the tip/sample heterostructure. In our case these are graphene, graphite and hBN (see Figure 8). A number of flakes are cataloged and revised in order to **design the final stack**. What we need to ensure in this step is that the dimensions of the flakes are compatible with each other and with the final substrate where they will be dropped.

Having the flakes ready is only half of the previous work needed to make a stack. It is also necessary to make the so called **stamp**. The stacking process is assisted by a thin film of polypropylene carbonate (PPC), a polymer that acts as adhesive layer. The stamp holds this PPC film and it is used to pick up the different flakes. Its morphology (see Figure 9a) includes two separate components: a **detachable PPC film** and a **reusable handle**.

3.2.2 Stacking process

With the stamp ready, and the heterostructure designed, we are in a good position to make the heterostructure. This whole process is carried out in the transfer station, an optical microscope specifically modified so the assembly of the heterostructures can be performed. The stacking is possible due to the adhesive properties of the PPC. Its interaction with the flake is strong enough to lift it from its original substrate. A subtle yet critical detail about the procedure is that the structure is **built from bottom to top**. This approach prevents the top surface from contacting any potential contaminating materials, such as PPC.

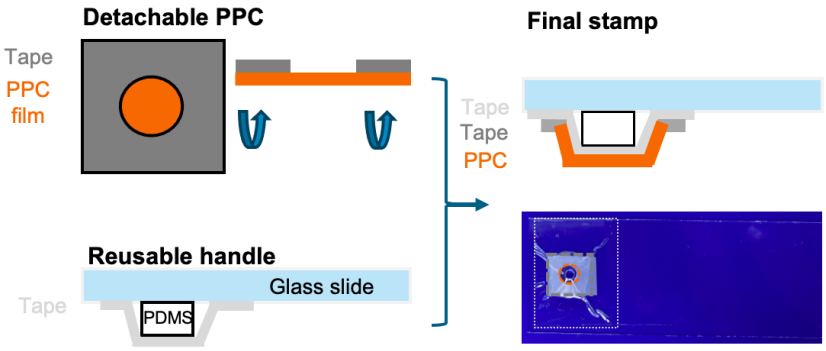

Figure 9: Morphology of the stamp to pick up the 2D materials: The detachable PPC is a thin film of PPC secured to a piece of scotch tape with a hole in the middle. The reusable handle is a glass slide with a piece of polydimethylsiloxane (PDMS) and clear tape over it. PDMS is a transparent polymer that can be squeezed very easily. Both parts are combined to obtain the final stamp. By doing so, we leverage from the adhesivity of the PPC and the viscoelastic properties of the PDMS to ensure a smooth pick up.

At the cost of having to detach the PPC film, and flip it before being able to drop the stack.

Now I will describe the process to build a heterostructure for a sample. In the simplest configuration, this stack is only formed by two flakes: hBN/graphene. Later on, I will highlight the differences if we also want to include a graphite flake at the bottom. Figure 10 shows some of the relevant steps of the pick up process.

- **Finding the touchdown point:** The first step is to find the spot of the stamp that will firstly touch the SiO_2 substrate. This is done by slowly lowering the stamp until the characteristic Newton rings are spotted.
- **hBN:** To pick up an hBN flake, the touch point can be placed directly over the hBN or a few tenths of microns away. The process starts by making contact with the stamp on the SiO_2 at 45ºC (figure 10a). The touching area is clearly recognizable by the change in the color, from purple to gray-ish, and its edge (the wavefront) is marked by the Newton rings. As the temperature is increased, the front advances. Figures 10 b and c show how the front passes through the flake as the temperature is controlled with the heater under the substrate. Once the whole flake has been covered, the temperature control is turned off. When the temperature reaches 25-28ºC, the stamp pops up and the flake stays on the PPC. Figure 10 shows an hBN flake that has been lifted from its original substrate.

- **Graphene:** When picking up the top layer, it is important to leave at least 10-15μm from one end of the flake to one of the edges of the hBN (see figure 10e where the graphene flake is outlined in red). The touch point in this case must be near the opposite edge of the hBN. The front advances by slowly increasing the temperature (see Figure 10f where the MLG is almost fully covered). The vdW forces the MLG feels from the hBN are stronger than the interaction with the SiO_2 so when we retract the front and lift the stamp, the graphene sticks to the hBN. This is done very slowly by decreasing the temperaure controll (Figure 10g). The pick is successful if we see an empty space where the flake used to be (Figure 10h).

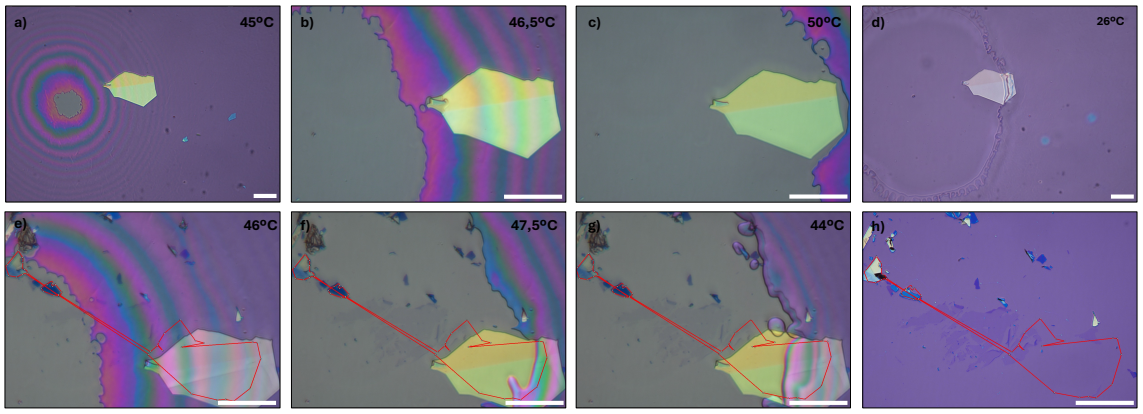

Figure 10: Images of the process to pick up an hBN flake (a-d) and a graphene flake (e-h). See main text for a detailed explanation of the steps. Scale bars are 50μm in all pictures.

If we wish to have a graphite flake as the bottom layer we must have prepared a slightly different stamp. In this case, the graphite flake is exfoliated directly on the PPC film and placed approximately at the center of the PDMS. This way, the graphite is already on the stamp and the first layer to be pucked up is still hBN. The reason for this is that, using PPC and the described method we were not able to consistently pick up graphite flakes.

3.2.3 Dropping the heterostructure and cleaning

Once the heterostructure has been stacked, we can detach it from the reusable handle simply pealing off the scotch tape. The drop down is assisted by a homemade handle that allows us to place the detachable PPC film on it and make contact with the final substrate. The process to drop a stack on a sample or on a tip is slightly different. Figure 11 shows the most important steps for both cases.

The homemade handle with the PPC on it is placed on the transfer station so its XYZ position can be controlled. The substrate's temperature is increased to 85ºC. Then, the PPC fume is slowly lowered with the Z microcontroller until contact is made (Figure 11a and d). When the stack has fully laid on the substrate, the wavefront is stopped and the temperature is increased to 130ºC. After a few moments at 130ºC, the PPC fume starts breaking (Figure 11b and e) and the arm can be lifted.

The next step is to vacuum anneal the device for 12h at 300ºC to get rid of the polymer and clean the surface. In the process, the PPC melts and the stack drifts away from its original position (see figure 11c where the stack has moved with respect to b). This is a big problem because **the drift is random and uncontrollable**. In the case of a sample, this issue can be overcome be evaporating the contacts after the annealing. However, it is a critical problem for the tip because the heterostructure always drifts away from the pyramid and the tip becomes useless. To solve this problem, we perform one final step before annealing a tip.

After the stack has been dropped on the pyramid, temperature is increased to 270ºC to start evaporating the PPC. At the same time, we use another AFM cantilever to hold the stack in position while the PPC melts (figure 11f). After some time enough PPC has been melted so the characteristic tent-like shape appears (Figure 11g).

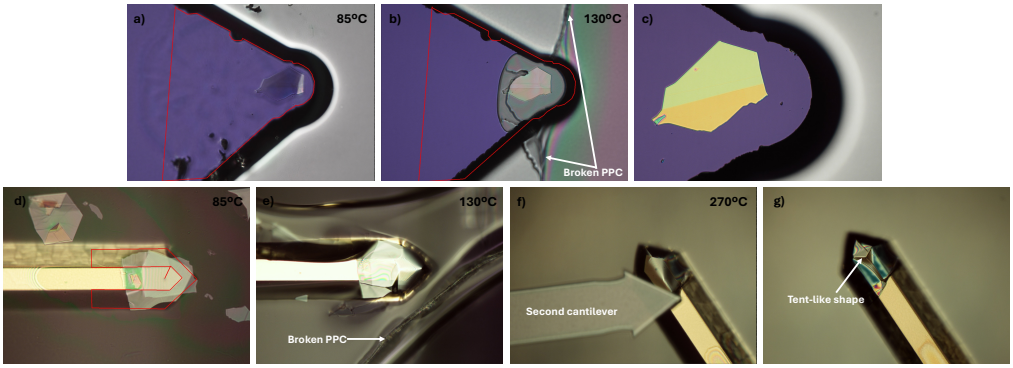

Figure 11: Process to drop a stack on a sample stage (a-c) and on a tip (d-g).

3.2.4 Electrical contacts

The final step of the fabrication is the evaporation of electrical contacts. In the simplest configuration, only the graphenes have contacts. However, it is also possible to evaporate contacts to the graphite flakes of both tip and sample to use them as top and bottom gates. In order to make the contacts, **standard lithography** plus evaporation methods are **not applicable to our case**. They require to cover the stack with photoresist which would contaminate the top surface.

Our initial approach then was to make electrical connections with prepatterned contacts, and drop the stack on top of them. However, the drift induced by the annealing made us discard this method, at least for the sample side. Too often the top layer ended up not touching the contacts and the sample had to be trashed. The solution we found was to fabricate a **physical (hard) mask** with the shape of the contacts. The mask is a Si chip where we have etched all the way through with the shape of an electrical contact. We then align the mask with the heterostructure and evaporate 5/50 nm of Cr/Au. The alignment is assisted by a commercial XYZ aligner that allows us to clamp the hard mask and sample together at the correct position. As a summary of the fabrication section, Figure 12 shows schematically the main steps to fabricate a sample with contacts to the graphite gate and graphene.

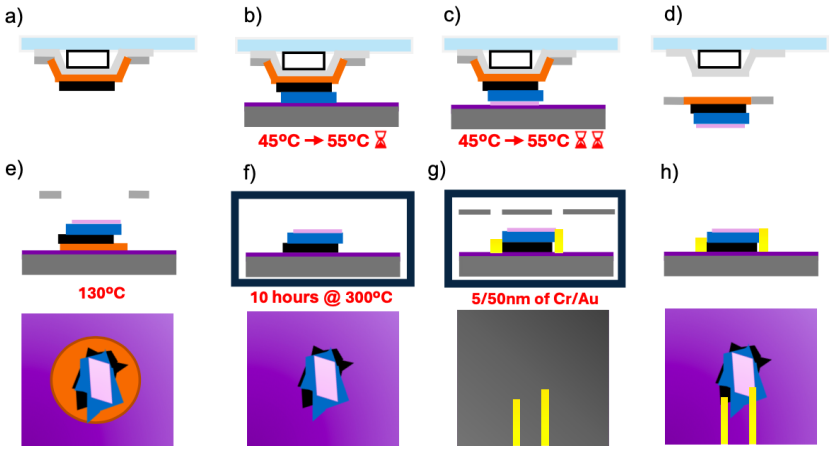

Figure 12: Steps to build a sample with a graphite gate. a) Starting point: stamp with graphite flake. b) Pick up of hBN. c) Pick up of graphene. d) Detachment of the PPC fume with the stack on it. e) Drop down of the heterostructure. f) Vacuum annealing. g) Contact evaporation. h) Final device.

4 Results and Discussion

In this section I present and discuss some of the experimental measurements we have performed with our QTM. I will firstly focus on the challenges that we have had to overcome to fabricate high quality tips and samples. Later, I will discuss our successful experiment that notably reproduces the key features expected in twistable bilayer graphene.

4.1 Challenges and preliminary measurements

Achieving the necessary quality standards for our fabrication techniques and instrumentation was crucial for reproducing the expected conductive characteristics. In order to obtain this measurement, we faced several fabrication and calibration challenges, primarily related to surface cleanliness and contact robustness. Before both of these topics were properly addressed, our measurements did not reproduce the expected behavior as can be seen in Figure 13.

The open surface nature of our heterostructures led us to anticipate that ensuring **highly clean surfaces** would be a critical issue that might impact our measurements. For this reason, we focused most of our efforts on achieving atomically clean surfaces. Working towards this goal we faced several challenges related to the stacking process:

- **Challenge:** Removing the polymer after dropping the stack. One of the most commonly used polymers as the adhesive layer to do the pick up is polycarboante (PC). Our main collaborating partners had great experience with this polymer but we could not benefit from their knowledge as PC requires to be dissolved using solvents. This solvents would contact the top surface and contaminate it. **Solution:** Using PPC, which gets removed by vacuum annealing.

- **Follow-up challenge:** No one at ICFO had experience working with PPC. **Solution:** Spending the necessary time to develop the right recipe to stack the materials. This took a lot of time since many parameters had to be optimize: size, shape and height of stamp, picking-up temperatures, annealing time...

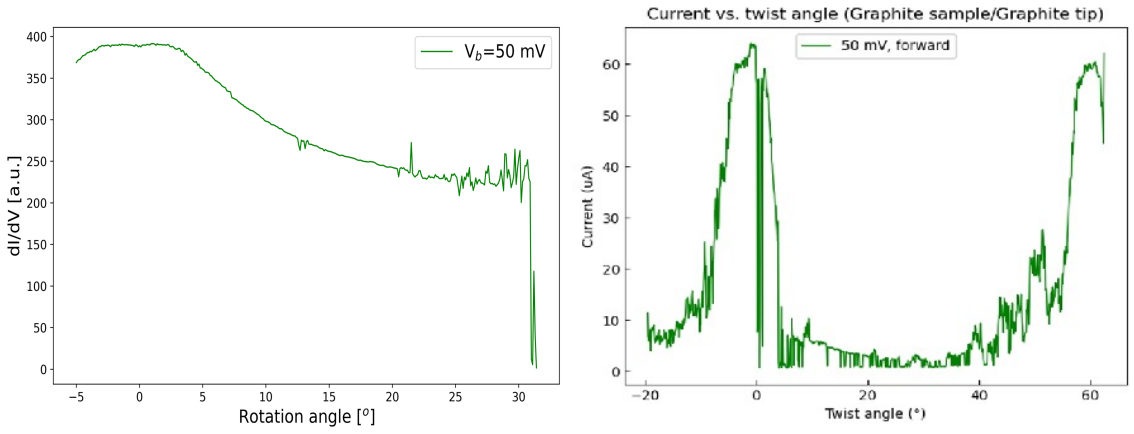

Figure 13: Preliminary measurements of two different pairs of tips and samples. The conductance (left) and current (right) are plotted as a function of the twist angle. Both quantities should following the same tendency and display the same features.

- **Challenge:** Never touching the the top surface with polymer to avoid contamination. **Solution:** Making the stack upside down and flipping it.
- **Follow-up challenge:** Flipping the heterostructure implies having the polymer as the bottom layer which induced drift during the annealing. This made us discard the initial plan of using pre-patterned contacts as the electrical connections to the layers. **Solution:** Using a hard mask to evaporate the gold contacts after the annealing. This took quite some time as no one at ICFO had experience fabricating these masks.

Ultimately, we optimized our process well enough to achieve the cleanness standards that were needed to perform in-situ twistronics experiments. A comparison between a clean and dirty sample can be seen in Figure 14. After this optimization process, which was instrumental for the success of the experiment, we realized that another aspect was negatively affecting the performance of the experiment: **the tip and sample contact robustness**. As can be seen in the right plot of Figure 13, the current drastically vanishes to zero at many angles. We identified that in these cases the problem was a partial detachment of the tip. To address this problem, we had to retract the tip, move it to another point and correct the tilt position of the sample with respect to the cantilever. With this fine alignment, the sudden drops in the signal could be minimized.

4.2 Successful experiment

The main result of this thesis is shown in Figure 15. This plot displays the conductance dI/dV as a function of the twist angle for a MLG tip and MLG sample. The measured conductance is approximately symmetric with respect to 30°, where it takes its minimal

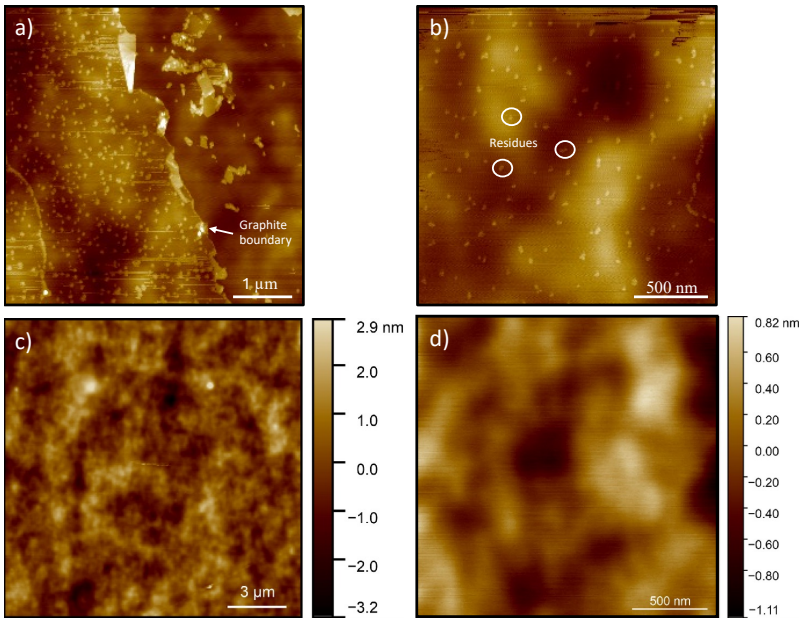

Figure 14: AFM images in non-contact mode of two different samples. a) 5x5 μm scan of a few layer graphite sample. An irregular line crosses diagonally the image corresponding to the boundary between the graphite (left) and hBN (right). b) Zoomed in image of the graphite side where clear signs of residues, probably PPC, are visible. c) 15x15 μm scan of a MLG sample with almost no sign of any kind of dirtiness. d) Zoomed in image of the same sample. The corrugation present in the sample is less than 2 nm which is very standard in these kind of heterostructures. These last two images confirm that with our recipe we achieve atomically clean surfaces.

value. From this point, it continuously raises as the angle increases (decreases) until it reaches a maximum close to 60° (0°). Additionally, two prominent conductance peaks appear at 21.85° and 38.08°.

The plateau observed at small angles and near 60° is due to the contact resistance, *i.e.* the resistance away from the tip. This resistive behavior limits the amount of current that can flow through the junction and sets a threshold for the measured conductance. On the other hand, the overall U-shape conductive behavior reflects an intrinsic property of the junction. In twisted BLG, interlayer hybridization is strongly suppressed for large angles ($|\theta| > 10°$) [21], thus the tunneling events between layers should be suppressed yielding a very low conductance. The measured data however, indicates that there must be another mechanism that triggers the overall angular dependency. As addressed by Koren *et. al* [18], the behaviour is compatible with a phonon-induced interlayer conductance. This kind of incoherent transport is driven by inelastic scattering of an electron with a beating mode phonon [22]. The phonons compensate the momentum mismatch between the Dirac cones of the top and bottom MLG thus creating a path between layers.

The angles where the conductive peaks appear correspond approximately to two of the six commensurate angles theoretically predicted for twisted bilayer graphene: $(30 \pm 8.2)°$ [21]. They also align with the previous work by Chari *et.al* [19], Koren *et. al* [18] and Inbar *et. al* [5]. At this commensurate angles, a super-cell is formed and the periodic structure becomes much larger. Specifically, the bilayer forms a $\sqrt{7} \times \sqrt{7}$ moiré cell in real space.

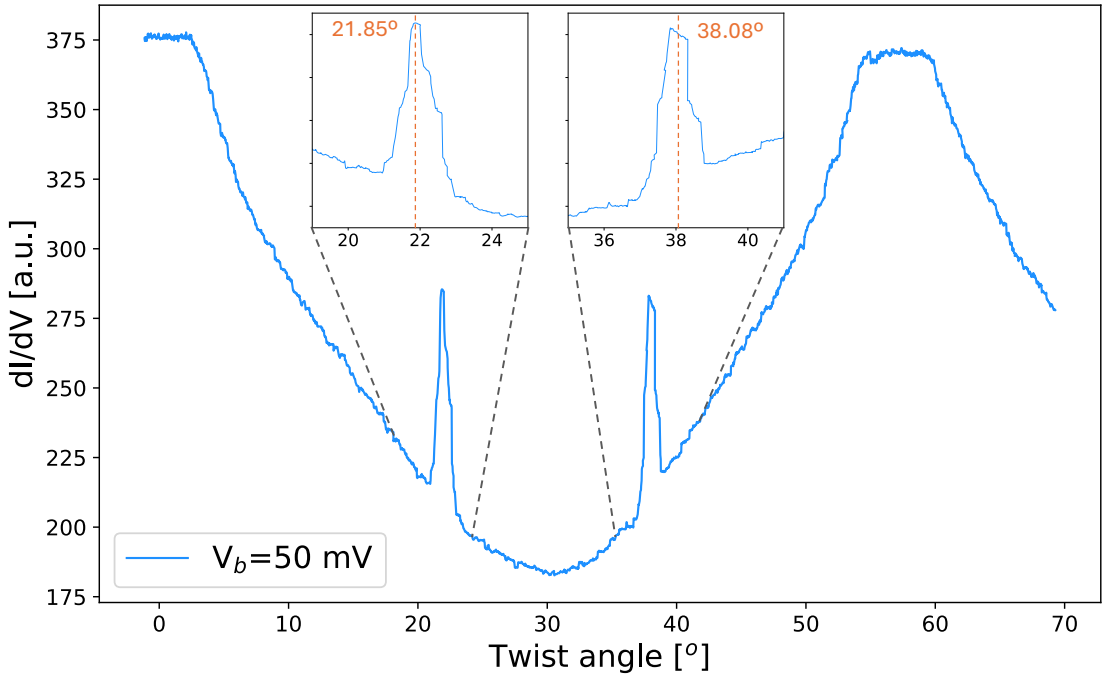

Figure 15: Measured conductance (dI/dV) as a function of the twist angle between a MLG tip and a MLG sample. The insets correspond to zoomed in images of the coherent peaks measured at 21.85° and 38.08°. The bias voltage created by the lock-in was 50 mV and the experiment was performed at room temperature.

To understand the nature of these peaks we need to recall that, a commensurate lattice in real space is also commensurate in momentum space. This implies that for commensurate stacking, there is a match in momentum of the electronic states of both layers (see Figure 16). For $\theta = 21.8°$ the Dirac cones of the two layers overlap at the third Brillouin zone. This fact is the essence of the coherent tunneling that causes the conductance peak. In comparison to an incoherent junction where electrons tunnel independently between layers at different locations to yield the overall current. The coherent interface is sensitive to the quantum mechanical behavior of the electrons and in this case the tunneling events at different position interfere coherently to give rise to an enhanced conductivity.

Figure 15 represents a big leap forward in or investigation. It demonstrates the capability of our setup to dynamically rotate two 2D crystals and measure the intrinsic electronic properties that arise. Having been able to reproduce all the key features previously reported for the twisted BLG interface validates the effectiveness of our experimental approach. However, more effort must be focused on repeating the experiment as we have not looked into reproducing systematically the data.

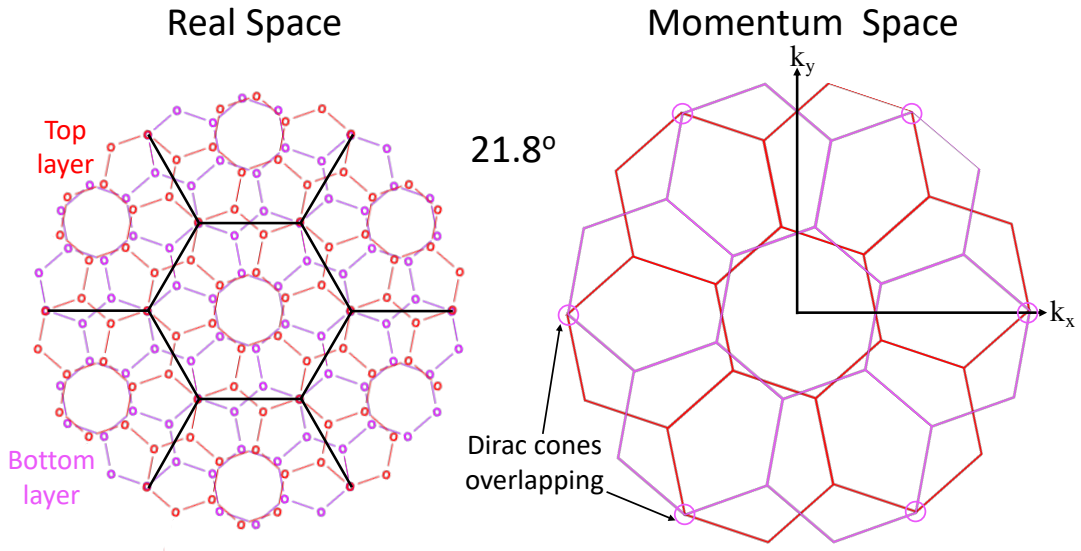

Figure 16: Representation of the real and momentum space of a bilayer graphene with a commensurate twist of 21.8°. In real space, the moiré unit vectors are $\sqrt{7}$ times bigger than the case of MLG. The black lines connect the positions where there is a perfect registry of atoms from both layers. In momentum space, there is also a commensurate periodicity. At the third Brillouin zone, 6 of the Dirac cones of both layers overlap indicating a match in momentum of the electronic states.

5 Outlook

Our investigation aims to further enhance the capabilities of the QTM by transforming it into an Quantum Twisting Optical Microscope (QTOM). This advanced system will enable the study of the opto-electronic properties of twistable junctions, providing new insights into the light-matter interactions in 2D materials.

The primary focus of this future work is to couple the QTM system to light and measure the absorption spectra of 2D interfaces. Specifically, we aim to study the near-infrared (NIR) and THz spectra of MATBG. This is of particular interest because the intra-flat band transitions of magic angle twisted bilayer graphene are known to lie within this spectral range [23, 24]. By investigating these transitions, we hope to gain a deeper understanding of the band structure of this fascinating and highly complicated system.

6 Conclusions

In this work, we have presented the current state of our Quantum Twisting Microscope, a novel scanning probe technique that allows for in-situ rotation of 2D crystals. To contextualize the novelty of the technique, the report began with an overview of 2D materials, focusing on moiré materials. This was followed by a review of the few experimental studies that have explored twistable 2D interfaces. We then delved into the operational principles of the QTM and described the in-situ twistronics experiment in detail. Given that this has been my main contribution to the project, a significant portion of the materials and methods section was devoted to describing the fabrication methods required to obtain the QTM tip and sample. Lastly, we presented our experimental results for the twistable BLG interface, highlighting the technical challenges that had to be overcome to achieve the expected behavior. We successfully reproduced the key features of the conductance as a function of the twist angle. It is particularly remarkable that we observed the commensurate peaks at 21.85° and 38.08°, demonstrating the capability of our setup to achieve coherent tunneling between layers at room temperature.

In conclusion, our journey to achieve successful in-situ twistronics measurements demonstrated the complexity and challenges inherent in fabricating and optimizing QTM experiments. Issues of sample cleanliness and tip-sample contact stability were critical obstacles that required innovative solutions and persistent efforts. The resulting fabrication method demonstrated highly clean surfaces which will be instrumental to the success of future experiments. Moreover, this fabrication technique is compatible with other SP experiments such as STM, so other research groups at ICFO will benefit from the optimized method. As we continue to refine and expand our experimental capabilities, the QTM will become a powerful tool to study the properties of other highly tunable systems by twist angle.

References

[1] Yuan Cao, Valla Fatemi, Shiang Fang, Kenji Watanabe, Takashi Taniguchi, Efthimios Kaxiras, and Pablo Jarillo-Herrero. Unconventional superconductivity in magic-angle graphene superlattices. *Nature*, 556(7699):43–50, 2018.

[2] Eric M Spanton, Alexander A Zibrov, Haoxin Zhou, Takashi Taniguchi, Kenji Watanabe, Michael P Zaletel, and Andrea F Young. Observation of fractional chern insulators in a van der waals heterostructure. *Science*, 360(6384):62–66, 2018.

[3] Hongyuan Li, Ziyu Xiang, Aidan P Reddy, Trithep Devakul, Renee Sailus, Rounak Banerjee, Takashi Taniguchi, Kenji Watanabe, Sefaattin Tongay, Alex Zettl, et al. Wigner molecular crystals from multielectron moiré artificial atoms. *Science*, 385(6704):86–91, 2024.

[4] Emma C Regan, Danqing Wang, Chenhao Jin, M Iqbal Bakti Utama, Beini Gao, Xin Wei, Sihan Zhao, Wenyu Zhao, Zuocheng Zhang, Kentaro Yumigeta, et al. Mott and generalized wigner crystal states in wse2/ws2 moiré superlattices. *Nature*, 579(7799):359–363, 2020.

[5] Alon Inbar, John Birkbeck, Jiewen Xiao, Takashi Taniguchi, Kenji Watanabe, Binghai Yan, Yuval Oreg, Ady Stern, Erez Berg, and Shahal Ilani. The quantum twisting microscope. *Nature*, 614(7949):682–687, 2023.

[6] Kostya S Novoselov, Andre K Geim, Sergei V Morozov, De-eng Jiang, Yanshui Zhang, Sergey V Dubonos, Irina V Grigorieva, and Alexandr A Firsov. Electric field effect in atomically thin carbon films. *science*, 306(5696):666–669, 2004.

[7] Yuanbo Zhang, Yan-Wen Tan, Horst L Stormer, and Philip Kim. Experimental observation of the quantum hall effect and berry's phase in graphene. *nature*, 438(7065):201–204, 2005.

[8] Luis EF Foa Torres, Stephan Roche, and Jean-Christophe Charlier. *Introduction to graphene-based nanomaterials: from electronic structure to quantum transport*. Cambridge university press, 2014.

[9] Alexander S Mayorov, Roman V Gorbachev, Sergey V Morozov, Liam Britnell, Rashid Jalil, Leonid A Ponomarenko, Peter Blake, Kostya S Novoselov, Kenji Watanabe, Takashi Taniguchi, et al. Micrometer-scale ballistic transport in encapsulated graphene at room temperature. *Nano letters*, 11(6):2396–2399, 2011.

[10] Ahmet Avsar, Jun You Tan, T Taychatanapat, J Balakrishnan, GKW Koon, Y Yeo, J Lahiri, A Carvalho, AS Rodin, ECT O'farrell, et al. Spin–orbit proximity effect in graphene. *Nature communications*, 5(1):4875, 2014.

[11] Yuan Cao, Valla Fatemi, Ahmet Demir, Shiang Fang, Spencer L Tomarken, Jason Y Luo, Javier D Sanchez-Yamagishi, Kenji Watanabe, Takashi Taniguchi, Efthimios Kaxiras, et al. Correlated insulator behaviour at half-filling in magic-angle graphene superlattices. *Nature*, 556(7699):80–84, 2018.

[12] Leon Balents, Cory R Dean, Dmitri K Efetov, and Andrea F Young. Superconductivity and strong correlations in moiré flat bands. *Nature Physics*, 16(7):725–733, 2020.

[13] J Diez-Merida, I Das, G Di Battista, A Diez-Carlon, M Lee, L Zeng, K Watanabe, T Taniguchi, E Olsson, and DK Efetov. High-yield fabrication of bubble-free magic-angle twisted bilayer graphene devices with high twist-angle homogeneity. *arXiv preprint arXiv:2405.11323*, 2024.

[14] Kevin P. Nuckolls and Ali Yazdani. A microscopic perspective on moiré materials, 2024.

[15] Ch. Gerber E. Weibel G. Binnig, H. Rohrer. Tunneling through a controllable vacuum gap. *Appl. Phys. Lett*, 70:178–180, January 1982.

[16] Sriram Sundararajan and Bharat Bhushan. Development of afm-based techniques to measure mechanical properties of nanoscale structures. *Sensors and Actuators A: Physical*, 101(3):338–351, 2002.

[17] D. W. Pohl, W. Denk, and M. Lanz. Optical stethoscopy: Image recording with resolution /20. *Applied Physics Letters*, 44(7):651–653, 04 1984.

[18] Elad Koren, Itai Leven, Emanuel Lörtscher, Armin Knoll, Oded Hod, and Urs Duerig. Coherent commensurate electronic states at the interface between misoriented graphene layers. *Nature nanotechnology*, 11(9):752–757, 2016.

[19] Tarun Chari, Rebeca Ribeiro-Palau, Cory R Dean, and Kenneth Shepard. Resistivity of rotated graphite–graphene contacts. *Nano letters*, 16(7):4477–4482, 2016.

[20] Bert Voigtländer. *Scanning probe microscopy: Atomic force microscopy and scanning tunneling microscopy*. Springer, 2015.

[21] Rafi Bistritzer and Allan H MacDonald. Transport between twisted graphene layers. *Physical Review B—Condensed Matter and Materials Physics*, 81(24):245412, 2010.

[22] Vasili Perebeinos, Jerry Tersoff, and Ph Avouris. Phonon-mediated interlayer conductance in twisted graphene bilayers. *Physical review letters*, 109(23):236604, 2012.

[23] Bingchen Deng, Chao Ma, Qiyue Wang, Shaofan Yuan, Kenji Watanabe, Takashi Taniguchi, Fan Zhang, and Fengnian Xia. Strong mid-infrared photoresponse in small-twist-angle bilayer graphene. *Nature Photonics*, 14(9):549–553, 2020.

[24] Simone Lisi, Xiaobo Lu, Tjerk Benschop, Tobias A de Jong, Petr Stepanov, Jose R Duran, Florian Margot, Irene Cucchi, Edoardo Cappelli, Andrew Hunter, et al. Observation of flat bands in twisted bilayer graphene. *Nature Physics*, 17(2):189–193, 2021.

A Mathematical explanation of lock-in filtering

The lock-in amplifier utilizes a technique called Phase-Sensitive Detection (PSD) to extract the desired signal from a noisy environment. The idea is to use a reference AC signal, with a reference frequency (ω_{ref}), to isolate the real measurement from the noisy signal. Inside the lock-in the following things occur to make this happen:

1. **Reference Signal**: The lock-in amplifier generates a reference signal, typically a sinusoidal waveform at a known frequency ω_{ref}:

$$V_{\text{ref}}(t) = V_{\text{ref}} \cos(\omega_{\text{ref}} t + \phi)$$

2. **Measured Signal**: The signal $V_{\text{sig}}(t)$ obtained from the experiment is usually a combination of the desired signal and noise:

$$V_{\text{sig}}(t) = V_{\text{sig}} \cos(\omega_{\text{ref}} t + \theta) + \text{noise}(t)$$

3. **Multiplication**: The lock-in amplifier multiplies the measured signal $V_{\text{sig}}(t)$ by the reference signal $V_{\text{ref}}(t)$:

$$V_{\text{mult}}(t) = V_{\text{sig}}(t) \cdot V_{\text{ref}}(t)$$

Using trigonometric identities, we get:

$$V_{\text{mult}}(t) = (V_{\text{sig}} \cos(\omega_{\text{ref}} t + \theta) + \text{noise}(t)) \cdot (V_{\text{ref}} \cos(\omega_{\text{ref}} t + \phi))$$

$$V_{\text{mult}}(t) = \frac{V_{\text{sig}} V_{\text{ref}}}{2} [\cos(\theta - \phi) + \cos(2\omega_{\text{ref}} t + \theta + \phi)] + \text{noise}(t) \cdot V_{\text{ref}}(t)$$

4. **Low-Pass Filtering**: The product $V_{\text{mult}}(t)$ consists of three components: one at the difference frequency (DC component), one at twice the reference frequency and a noisy component which we can neglect:

$$V_{\text{mult}}(t) = \frac{V_{\text{sig}} V_{\text{ref}}}{2} \cos(\theta - \phi) + \frac{V_{\text{sig}} V_{\text{ref}}}{2} \cos(2\omega_{\text{ref}} t + \theta + \phi)$$

A low-pass filter is used to remove the high-frequency component $\cos(2\omega_{\text{ref}} t + \theta + \phi)$, leaving only the DC component:

$$V_{\text{filtered}} = \frac{V_{\text{sig}} V_{\text{ref}}}{2} \cos(\theta - \phi)$$

By removing the high-frequency term, the lock-in amplifier isolates the desired signal at the reference frequency, providing a clean measurement of V_{sig}. This process effectively filters out the noise, ensuring accurate and precise signal detection.